# Rolling and recrystallization textures of bcc steels

**Martin Hölscher, Dierk Raabe and Kurt Lücke**

The rolling and recrystallization texture development of bcc steels is discussed for three examples belonging to three different types of steels, namely deep drawing steels (e.g. low carbon steel), ferritic stainless steels (e.g. Fe16%Cr) and electrical steels (e.g. Fe3%Si).

**Walz- und Rekristallisationstexturen kubisch raumzentrierter Stähle.** Die Entwicklung der Walz- und Rekristallisationstexturen kubisch raumzentrierter Stähle wird anhand dreier verschiedener Stahlsorten mit unterschiedlichen technischen Anforderungen dargestellt: Niedriggekohlte Tiefziehstähle, ferritische Chromstähle (Fe16%Cr) und Transformatorstähle (Fe3%Si).

The rolling and recrystallization textures of the different types of bcc steels often show great similarities, but also exhibit characteristic differences which, e.g. depend upon starting texture, microstructure and condition of precipitations. In this paper this behaviour will be discussed for three examples belonging to three entirely different types of steels.

**Deep-drawing steels (e.g. low-carbon steel).** Here the most important property is a good deformability in deep drawing. This behaviour is favoured by a texture formed in such a way that during deep drawing the material flow occurs from the width and not from the thickness of the sheet and that it is equal for different directions in the sheet plane, i.e. by materials with the high $r$-value and a low $\Delta r$-value ($r$ is the Lankfort parameter). Both properties can be achieved by a texture which after recrystallization consists of a homogeneous strong fibre texture with a {111} plane parallel to the sheet plane.

**Ferritic stainless steels (e.g. Fe16%Cr).** Here again the requirements for deep drawability should be fulfilled, but additionally the ridging which often occurs in Cr-steels should be suppressed. This again means a {111} fibre texture but also a topologically random arrangement of crystallites should be achieved[1]).

**Electrical steels (e.g. Fe3%Si).** For the use of these steels in transformers high magnetic permeability for magnetisation in rolling direction is required which can be obtained by a ⟨100⟩ direction parallel to the rolling direction. Technologically this can be achieved by forming a very sharp Goss texture {011}⟨100⟩ by secondary recrystallization.

**Table 1** summarizes the textural requirements for these steels. As will be shown, the differences in the rolling and recrystallization textures of these various steels largely originate from differences in microstructure and texture of the hot-rolled band, **table 2.**

## Description of bcc textures

In order to demonstrate textures in bcc metals, mostly {110} pole figures are measured because they yield the highest X-ray intensity. Although being commonly used such pole figures impose great difficulties on the quantitative interpretation of textures, since the superposition of the considered types of poles leads to a high degree of ambiguity. To obtain a less ambigous description, the orientation distribution function (ODF) must be calculated. It is mostly presented in the three-dimensional orientation space in which a orientation $g$ is given by the three eulerian angles $\varphi_1$, $\Phi$ and $\varphi_2$. In the present paper the ODF is reproduced from 3 to 4 different pole figures (110, 200, 112, 103) by the series expansion method ($l_{max} = 22$) and is represented in the sections $\varphi_1 = 0°, 5°, \ldots, 90°$ through the eulerian space[2]), **figure 1.**

The rolling and recrystallization ODFs of bcc steels are mostly composed of certain orientation fibres and their main features can thus be represented in a very condensed manner by plotting the orientation density along these fibres[3])–[5]). The most important of these fibres appear as straight lines in the Euler angle space and are shown in **figure 2:**

$$\alpha\text{-fibre } \langle 110\rangle \,||\, \mathrm{RD} \quad \{001\}\langle 110\rangle \text{ to } \{111\}\langle 110\rangle, \qquad (1)$$

$$\gamma\text{-fibre } \{111\} \,||\, \mathrm{ND} \quad \{111\}\langle 110\rangle \text{ to } \{111\}\langle 112\rangle, \qquad (2)$$

$$\eta\text{-fibre } \langle 001\rangle \,||\, \mathrm{RD} \quad \{100\}\langle 001\rangle \text{ to } \{110\}\langle 001\rangle. \qquad (3)$$

In certain textures some peaks in the ODF cannot be shown by the fibres because of their static coordinates. Then the β-fibre which is a skeleton line and comprises the

**Table 1.** Textural requirements for various steels

**Tafel 1.** Anforderungen an die Textur verschiedener Stähle

| Steel | desired properties | required texture |
|---|---|---|
| 1) deep-drawing steels (low carbon) | good deformability<br>high $r$-value (Lankford parameter)<br>isotropic deformation<br>low $\Delta r$-value | {111} fibre texture with parallel normal direction |
| 2) ferritic stainless steels (e.g. Fe16%Cr) | good deformability as in (1)<br>avoiding of ridging and raping | {111} parallel normal direction<br>topologically random distribution of grains |
| 3) electrical steels (e.g. Fe3%Si) | low magnetic losses<br>high permeability in rolling direction | ⟨100⟩ parallel rolling direction (e.g. Goss-texture {011}⟨100⟩) |

*Dr.-Ing. Martin Hölscher,* Betriebsingenieur, Werkstoffentwicklung, Stahlwerke Peine-Salzgitter AG; *Dipl.-Ing. Dierk Raabe,* assistant; *Professor Dr. rer. nat. Dr. h. c. Kurt Lücke,* director emeritus, Institut für Metallkunde und Metallphysik, RWTH Aachen, Germany.

**Table 2.** Microstructure and texture of rolled steels

**Tafel 2.** Mikrostruktur und Textur gewalzter Stähle

| | | Low carbon steel | Alloyed steels Fe16%Cr, Fe3%Si |
|---|---|---|---|
| Hot rolling | micro-structure | 100% transformation $\gamma \rightarrow \alpha$ small globular grains | inhomogeneous through thickness: *center:* flat, strongly deformed grains, not recrystallized *surface:* grains very large, esp. for Fe3%Si |
| | texture | homogeneous through thickness; nearly random | very inhomogeneous through thickness *center:* strong rolling texture, $\alpha$-, $\gamma$-fibre *surface:* shear texture {011}⟨100⟩, ≈ {112}⟨111⟩ |
| Cold rolling | micro-structure | rolling degrees >80%: shear bands increasing with increasing amount of solute carbon or grain size | |
| | texture | increase of $\alpha$- and $\gamma$-fibre orientations: *rolling degrees <75%:* {112}⟨100⟩, $\alpha$ {111}⟨112⟩, $\gamma$ *rolling degrees >75%:* {111}⟨110⟩, $\alpha$, $\gamma$ | inhomogeneous due to starting texture *center:* sharpening of hot rolling texture, increase of {112}⟨110⟩, $\alpha$ and of {111}⟨110⟩, $\alpha$, $\gamma$ *surface:* increase of $\alpha$- and $\gamma$-fibre orientations (see low carbon steels), but much stronger {001}⟨110⟩ |
| Recrystallization | micro-structure | rolling degree <80%: first recrystallized grains in shear bands, grains with strong work hardening ({111}\|\| ND) recrystallized first | |
| | texture | strong decrease of the $\alpha$-fibre orientations (without {111}⟨110⟩, increasing density of Goss-orientation with increasing amount of shear bands, sharp rolling texture component {112}⟨110⟩ leads to a sharp recrystallization texture component {111}⟨112⟩ | |

true maxima of all sections along $\varphi_1$ and thus having variable $\varphi_2$ and $\Phi$ coordinates, has to be applied.

## Model calculations of bcc rolling textures

For the description of the rolling textures of bcc steels both experimental results as well as Taylor model calculations suggested the use of the $\alpha$-fibre. The use of the $\gamma$-fibre, however, was controversial for some time since for this purpose another fibre, the so-called $\beta$-fibre, was also discussed. This fibre was a result of first calculations of texture development according to the Taylor full constraints model of polycrystalline deformation which, additionally to the $\alpha$-fibre, predicted a fibre running from {112}⟨110⟩ to about {11 11 8}⟨4 4 11⟩. **Figure 3** shows that both combinations, $\alpha$ and $\gamma$ or $\alpha$ and $\beta$, are able to describe the pole figures of the rolling texture shown in figure 1, but the ODF representation of **figure 4** exhibits the better fit of the combination $\alpha$- and $\gamma$-fibre in case of deformation textures. The $\beta$-fibre, however, is today more often used for the description of certain recrystallization textures.

The reason for the deviation from the original Taylor model is connected with the gain shape. The original "full constraints" Taylor model allows plane strain for the various grains only of the size of the macroscopic strain of the specimen[6)7)]. The ODFs resulting from this model for different strains are shown in the first line of **figure 5.** In this figure sections $\varphi_2 = 45°$ of the ODFs are chosen since they happen to contain both the $\alpha$- and $\gamma$-fibre (see figure 2). The orientations of the $\beta$-fibre {112}⟨110⟩ and {11 11 8}⟨4 4 11⟩ (8° below {111}⟨112⟩ at $\varphi_1 = 90°$) are clearly preferred. But during rolling the initially more or less equiaxed grains become flat which allows a shear $\varepsilon_{13}$ parallel to the sheet plane in rolling direction, since for such band-shaped grains the incompatible deformation between neighbouring grains due to the $\varepsilon_{13}$ shear then appears only at their smallest edge and thus may only influence a small seam of the grains. This relaxed constraints model, which, additionally to plane strain also allows the shear $\varepsilon_{13}$, is called lath model. In the texture simulations for this case the main orientation is shifted to the exact position of {111}⟨112⟩ on the $\gamma$-fibre as can be seen in figure 5. After further deformation and flattening of the grains shear $\varepsilon_{23}$ also becomes possible without compatibility problems which would lead to the texture shown in the third line of figure 5. Finally, simultaneous relaxation of both shears lead to a texture as shown in the last line of figure 5. This so-called pancake model gives quite a homogeneous orientation density along the $\gamma$-fibre[8)9)].

In carrying out model calculations an often neglected parameter is the starting texture. In case of a non-random starting texture it is useful to consider the rate of rotation of the various orientations of the grains during rolling deformation. As an example in **figure 7** the angle calculated by the Taylor full constraints model for a rolling reduction of 10% is plotted for the section $\varphi_1 = 0$. The very slowly rotating regions are hashed. Although here {11 11 8} ⟨4 4 11⟩ is the only stable end orientation, the two orientations {112}⟨110⟩ and {001}⟨110⟩ do nearly not rotate at all, i.e. they are metastable. All orientations which first rotate towards one of these two positions will be fixed there.

## Experimental investigations of rolling texture development

In **figure 6** the transition from the Taylor full contraints model to the pancake model, in which all shears parallel to the rolling plane are relaxed in the course of rolling, is shown for an experimental example (Fe16%Cr). There one sees that with increasing degree of rolling the orientation of the main component at {11 11 8}⟨4 4 11⟩ is shifted to {111}⟨112⟩. This transition is characteristic for all steels investigated. The main reason for the differences in the texture development of the here considered three types of steels lies in the hot-rolling textures which act as starting textures. Hot rolling of the low carbon steel takes place

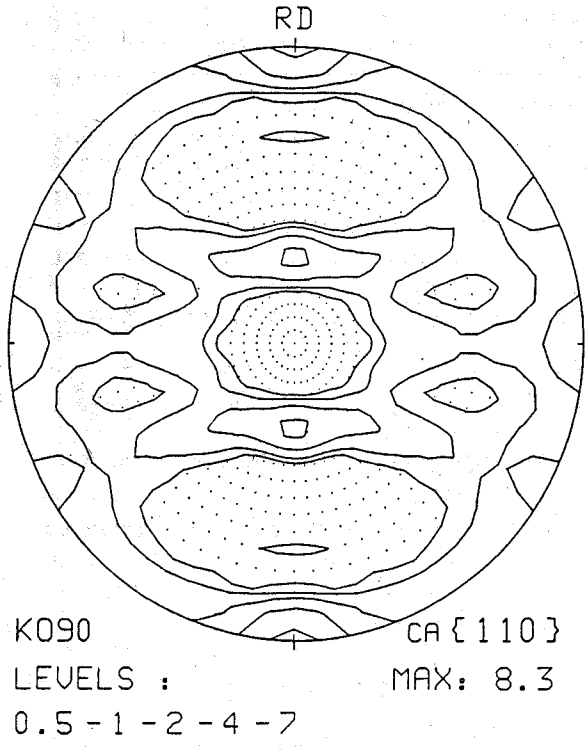


**Figure 1.** Rolling texture of a bcc steel ($\varepsilon$ = 90%)

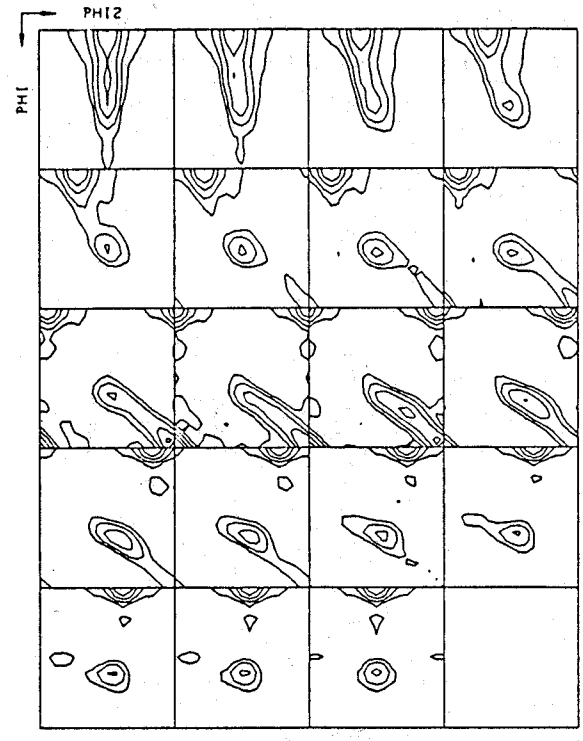


**Bild 1.** Walztextur eines kubisch-raumzentrierten Stahles ($\varepsilon$ = 90%)

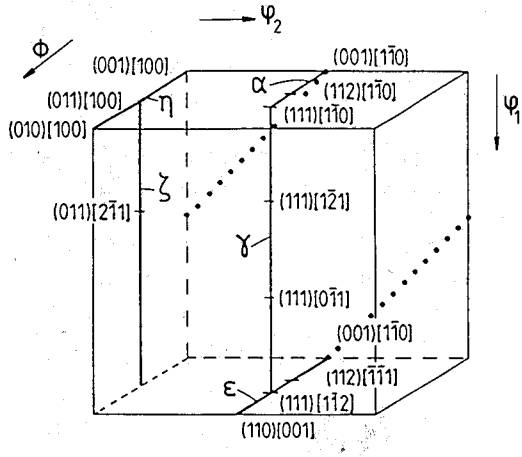


**Figure 2.** Reduced Euler space with fibres

**Bild 2.** Reduzierter Eulerraum mit einigen Fasern

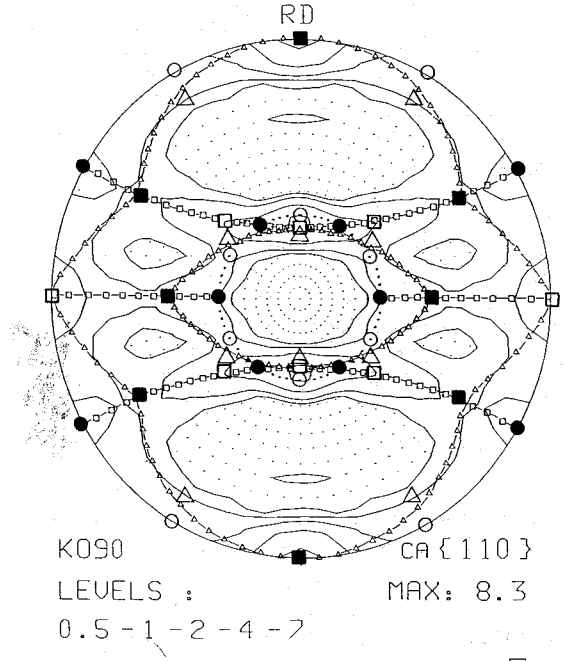


**Figure 3.** Fibres in a pole figure

**Bild 3.** Fasern in einer Polfigur

□ : α-fibre
△ : β-fibre
○ : γ-fibre

completely in the austenitic range. The subsequent transformation during cooling to ferrite results in a nearly random texture, **figures 8a, 9.** In the two alloyed steels Fe16%Cr and Fe3%Si, in contrast, the ferrite is stabilized up to the hot-rolling temperatures so that, since dynamic recovery during hot rolling prevents recrystallization, the deformation texture is present in the hot-rolled material essentially contains the cold-deformation textures; e.g. Fe16%Cr, **figures 8b, 10.** Due to the rolling conditions the ranges near the surface are deformed by shear and those near the center by nearly plane strain. The shear texture of the surface consists of a strong Goss texture {011}⟨100⟩ and of approximately {112}⟨111⟩. The texture in the center is similar to a cold-rolling texture with a strong α-fibre, especially {001}⟨110⟩, and a γ-fibre[10)11)].

Concerning the development of the cold-rolling texture, **figure 11,** the low-carbon steel exhibits a good agreement with the model calculations. The α-fibre increases continuously and in the γ-fibre {111}⟨112⟩ is dominant up to a

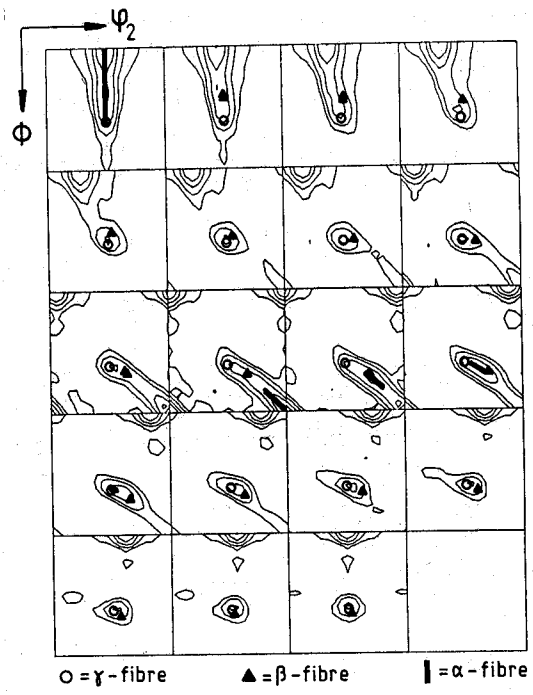


**Figure 4.** Fibres in the Euler space

**Bild 4.** Fasern im Eulerraum

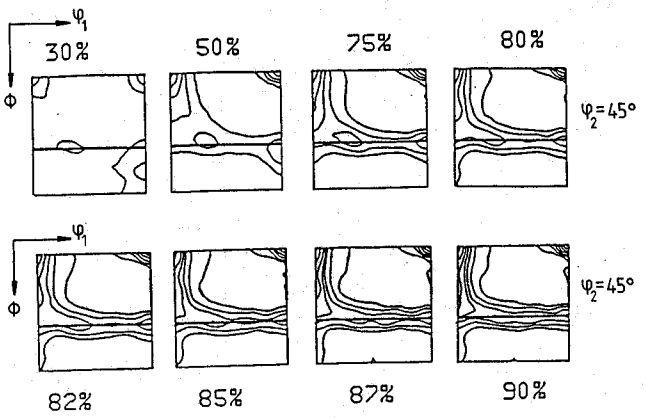


**Figure 6.** Experimental data of the cold rolling development in $\varphi_2 = 45°$ sections

**Bild 6.** Experimentelle Daten der Kaltwalztexturentwicklung in $\varphi_2 = 45°$-Schnitten

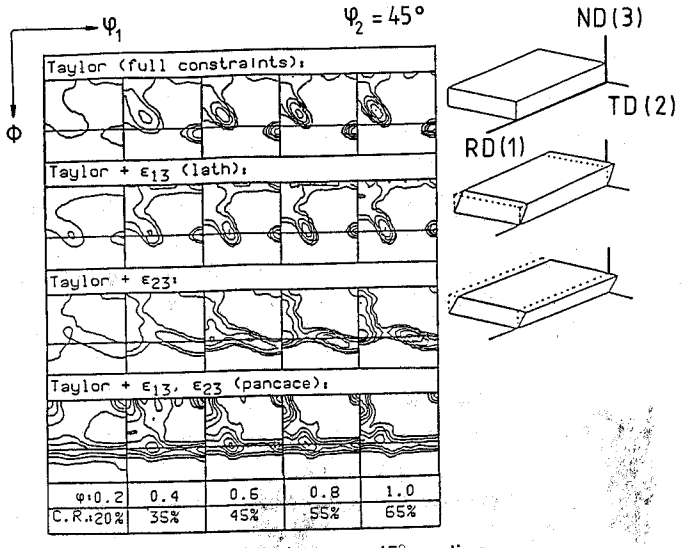


**Figure 5.** Taylor models in $\varphi_2 = 45°$ section

**Bild 5.** Taylor-Modell in $\varphi_2 = 45°$-Schnitten

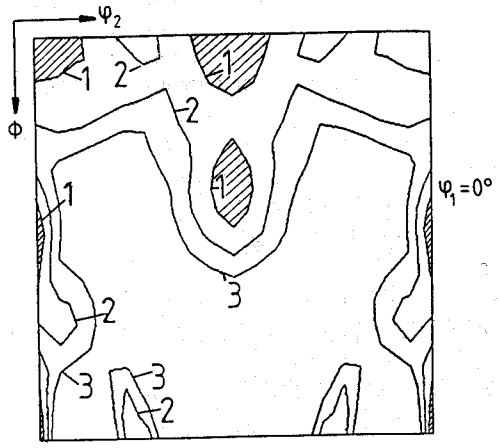


**Figure 7.** Rotation velocities in the $\varphi_1 = 0°$ section

**Bild 7.** Drehgeschwindigkeit im $\varphi_1 = 0°$-Schnitt

**Figure 8b.** Surface and center hot-rolling texture of Fe-16%Cr steel

**Bild 8b.** Warmwalztextur von Oberfläche und Mitte eines Fe16%Cr-Stahls

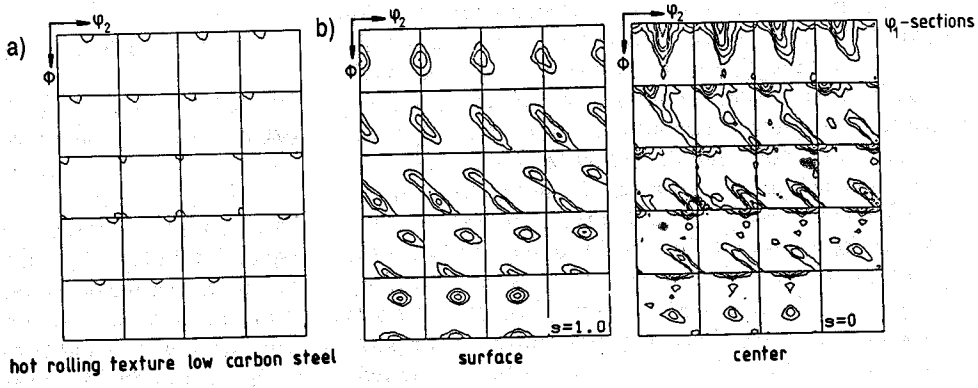


**Figure 8a.** Hot-rolling texture of a low-carbon steel

**Bild 8a.** Warmwalztextur eines niedriggekohlten Tiefziehstahls

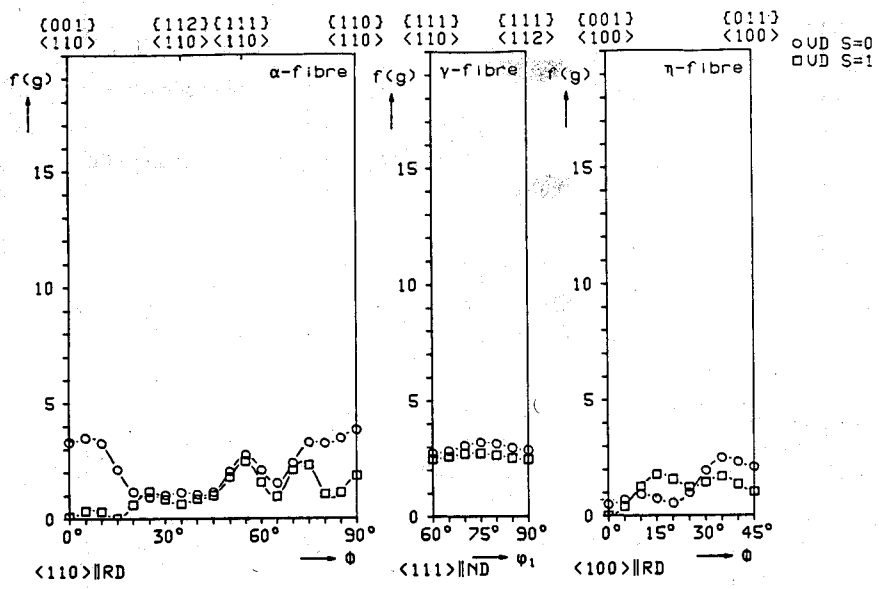


**Figure 9.** Fibres of hot-rolling texture of a low-carbon steel

**Bild 9.** Fasern der Warmwalztextur eines Tiefziehstahls

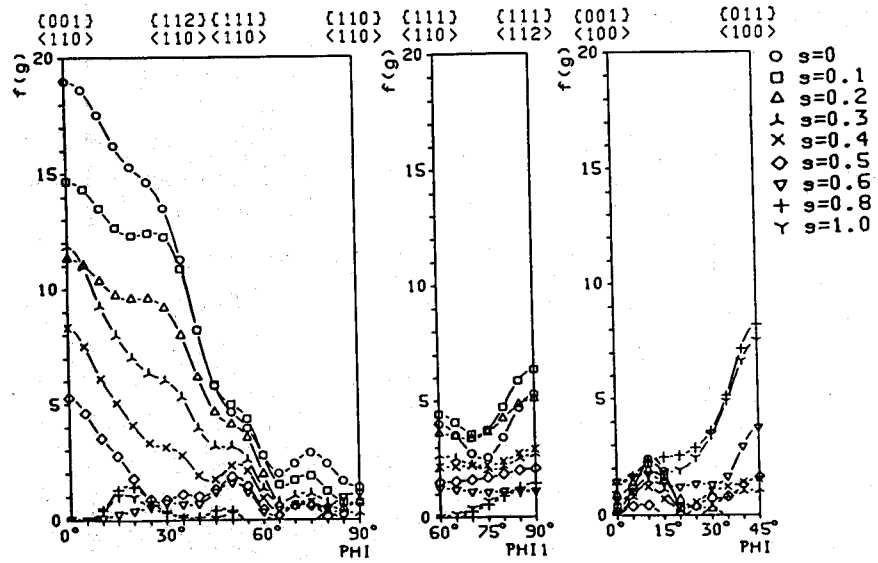


**Figure 10.** Fibres of hot-rolling texture of Fe-16%Cr

**Bild 10.** Fasern der Warmwalztextur von Fe-16%Cr

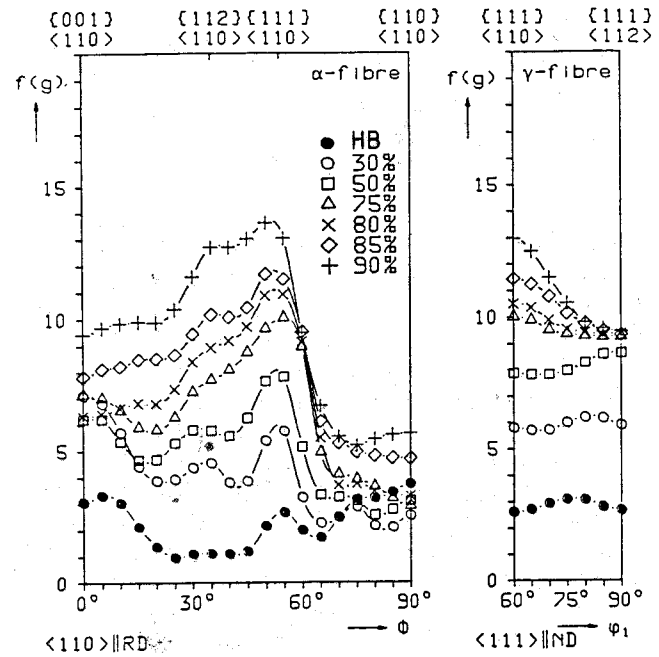


**Figure 11.** Cold-rolling texture of a low-carbon steel, C in solution

**Bild 11.** Kaltwalztextur eines Tiefziehstahles mit C in Lösung

rolling degree of 70% (lath model, shear $\varepsilon_{13}$) and {111}⟨110⟩ for higher rolling degrees (pancake model, additionally shear $\varepsilon_{23}$). In the deformation range between 70 and 80% strong shear band formation takes place in the {111}⟨112⟩ grains which is probably responsible for the relatively weak increase of texture sharpness.

Despite of the quite different starting conditions the cold-rolling textures of the alloyed steels show a rather similar development. At the surface, **figure 12a,** again first {111}⟨112⟩ and then, after 75%, {111}⟨110⟩ increases. The strongest difference is observed for the orientation density at {001}⟨110⟩ which is here much stronger than for the low-carbon steels because of the 35° rotation of the shear orientation {112}⟨111⟩ around the transverse direction. The starting texture for the center is nearly a cold-rolling texture and microstructure with elongated flat

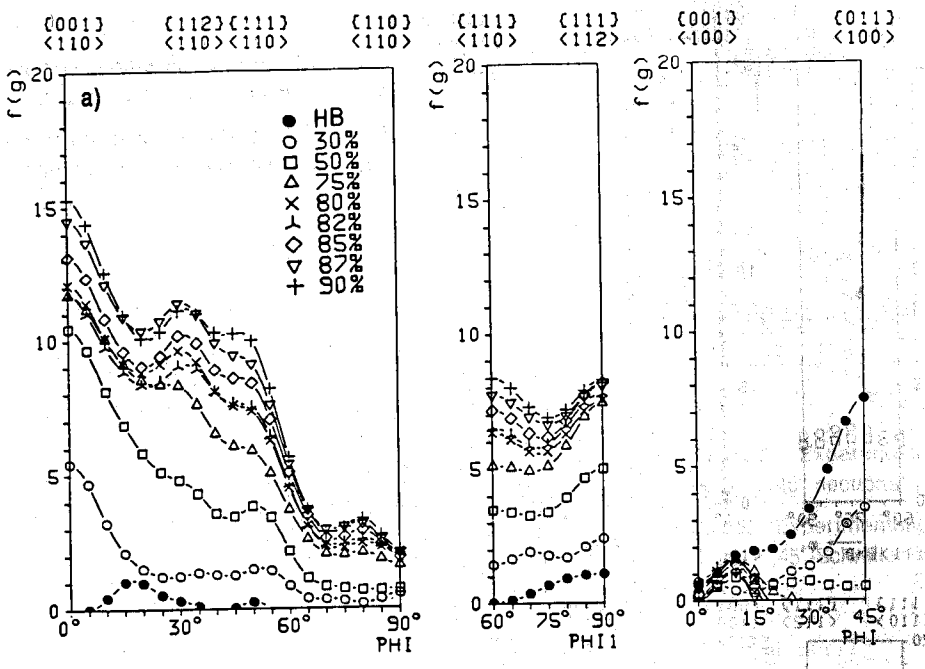


**Figure 12a.** Cold-rolling texture FeCr/FeSi surface

**Bild 12a.** Kaltwalztextur FeCr/FeSi Oberfläche

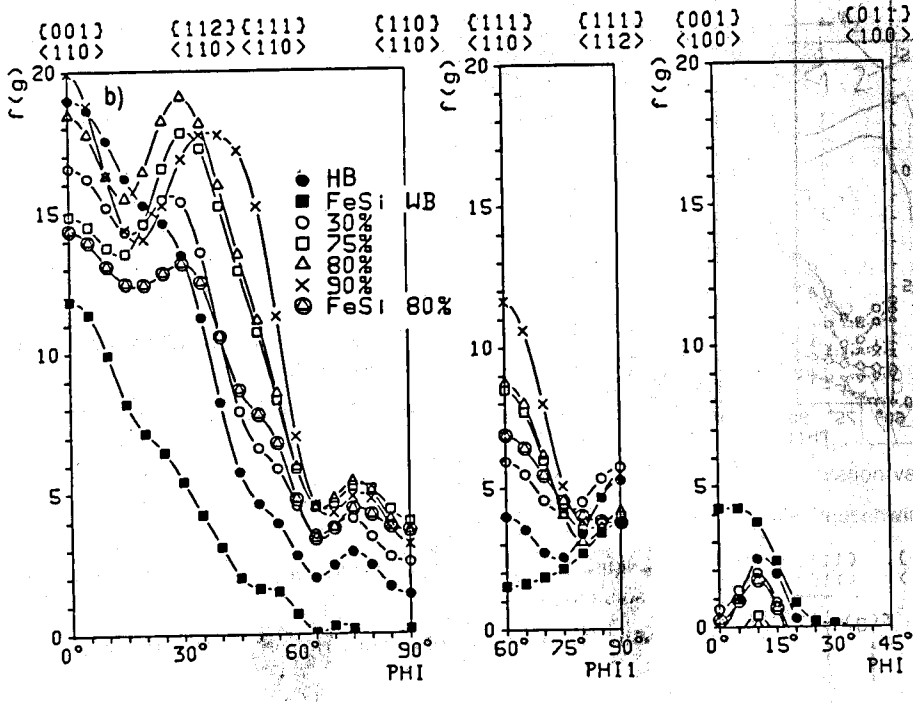


**Figure 12b.** Cold-rolling texture FeCr/FeSi center

**Bild 12b.** Kaltwalztextur FeCr/FeSi Mitte

grains. This means that the pancake model is valid for the texture development already from the beginning of cold rolling which means, that from beginning {111}⟨110⟩ is the most important orientation of the $\gamma$-fibre, **figure 12b.** The relaxed constraints models are thus able to rather well describe the texture development of quite different steels.

## Recrystallization textures

The recrystallization textures of the low-carbon steel, **figure 13,** exhibits the most characteristic feature of the development of recrystallization textures being generally valid for ferritic steels: the orientation density of the $\alpha$-fibre, in particular of the strong rolling texture component {112}⟨110⟩ decreases nearly to unity. This can be seen by comparison with figure 11. Only the orientation {111}⟨110⟩ simultaneously belonging to the $\alpha$- and $\gamma$-fibre remains rather strong after recrystallization.

As can be seen in **figure 14** for low degrees of rolling, the recrystallization randomizes the whole texture. With increasing degree of rolling, annealing leads to growth of the orientations of the $\eta$-fibre, expecially of the Goss orientation {011}⟨100⟩. High rolling degrees, finally, strengthen the $\gamma$-fibre and diminish the $\eta$-fibre. Both kinds of recrystallization texture development may be understood by combination of oriented growth and oriented nucleation. At the beginning of recrystallization it is possible to see in metallography, as also checked by TEM analysis, the $\gamma$-fibre grains appear to be hashed and the $\alpha$-fibre grains to be bright. After 10 s annealing strong nucleation took place, but only in the striped grains, i.e. in the $\gamma$-fibre, which have a high dislocation density and a high Taylor

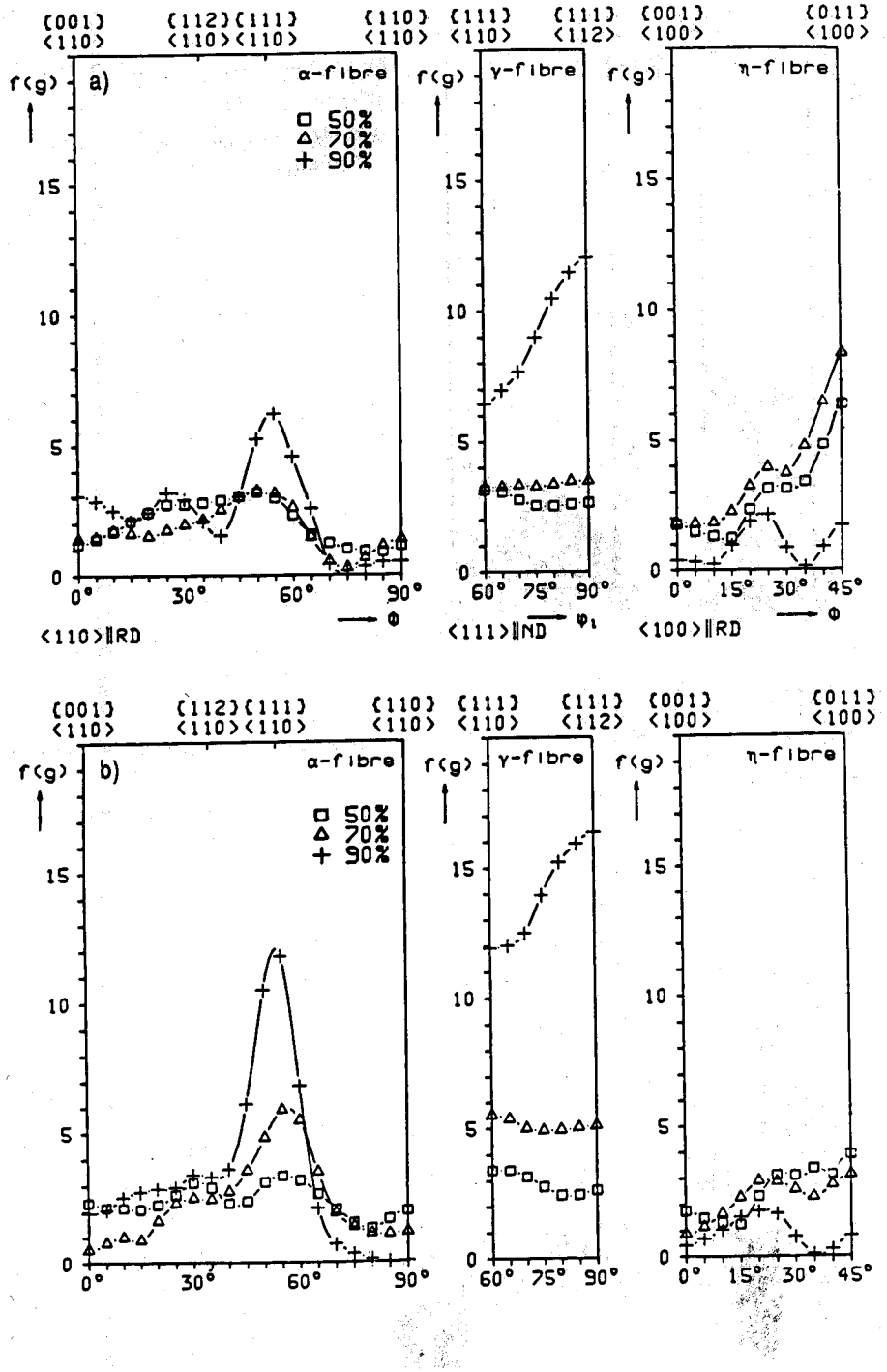


**Figure 13.** Recrystallization texture of a low-carbon steel, C in solution

**Bild 13.** Rekristallisationstextur eines Tiefziehstahles mit C in Lösung

factor, whereas no nuclei could be found in $\alpha$-fibre grains. Since at this stage the $\gamma$-fibre orientations still show the same intensity as the rolled material, it must be concluded that also the microscopically visible nuclei posses the same $\gamma$ orientations as the cold-rolled material, **figure 15.** On the other hand, it is of major importance that between the $\alpha$-orientation $\{011\}\langle 211\rangle$ and the rolling texture component $\{111\}\langle 112\rangle$ one has an orientation relationship of 35° around the $\langle 110\rangle$ transverse direction. This is close to the ideal orientation relationship of 27° $\langle 110\rangle$ found for high growth rates found in the bi-crystal experiments by Ibe and Lücke[12])[16]) and allows growth of the $\gamma$-fibre nuclei into the $\alpha$-fibre grains. Taking into consideration the formation of $\{111\}\langle uvw\rangle$ oriented nuclei in the $\gamma$-fibre on the basis of a $30°\langle 111\rangle$ rotation[14]), as well as the $35°\langle 110\rangle$ orientation relationship, the typical recrystallization texture with a maximum at $\{111\}\langle 112\rangle$ can be explained by a combination of oriented nucleation and oriented growth. A striking example for a recrystallization texture, which is mainly formed by oriented growth is given in **figures 16 and 17.** Here the maximum in the recrystallization texture is at $\approx\{557\}\langle 583\rangle$ which indeed has an ideal $27°\langle 110\rangle$ relationship to $\{112\}\langle 110\rangle$. In this case Zener drag is supposed to deteriorate the mobility of the non-special boundaries, whereas the special $27°\langle 110\rangle$ boundary is not influenced by particles[13])[15]). Nearly the same fast growth relationship exists between Goss and the rolling component $\{111\}\langle 112\rangle$. This principally explains the occurrence of the Goss component in the recrystallization texture. Its nucleation is assumed to take place in shear bands, rotated 35° around the transverse direction. The amount of goss increases with deformation since the $\{111\}\langle 112\rangle$ compo-

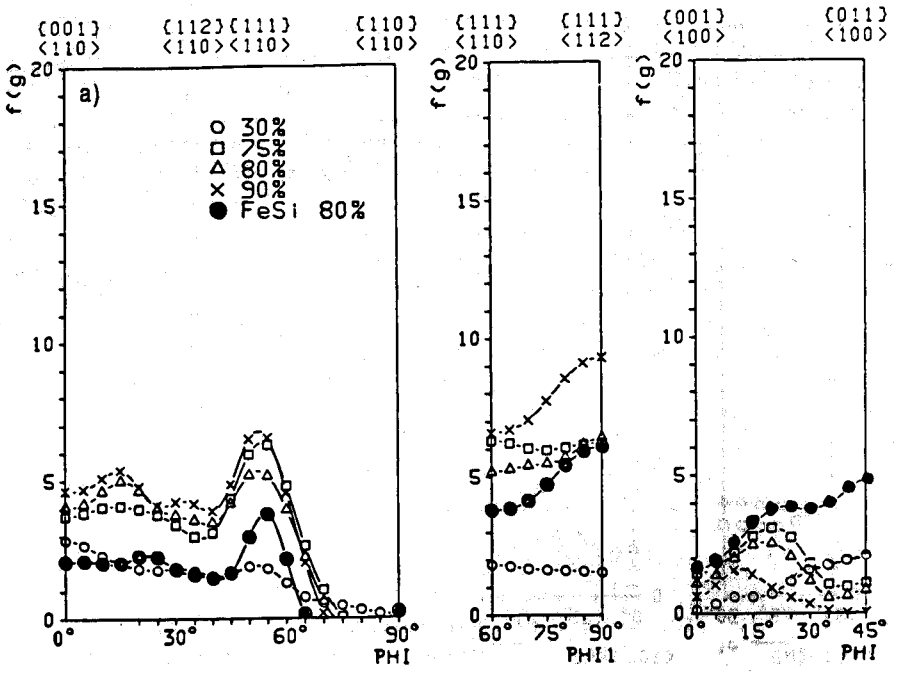


**Figure 14a.** Recrystallization texture FeCr/FeSi surface

**Bild 14a.** Rekristallisationstextur FeCr/FeSi an der Oberfläche

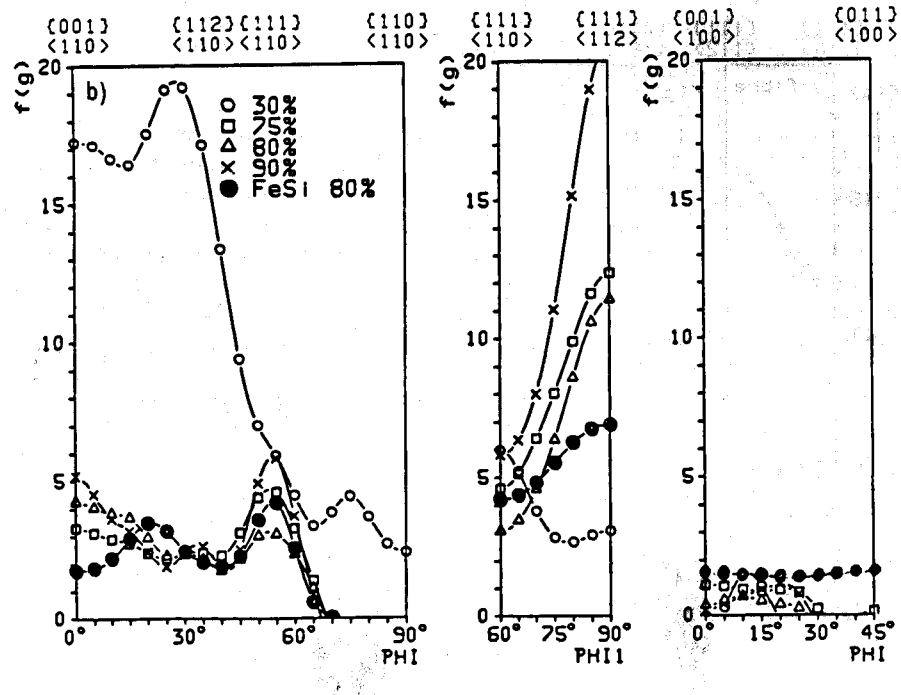


**Figure 14b.** Recrystallization texture FeCr/FeSi center

**Bild 14b.** Rekristallisationstextur FeCr/FeSi in der Mitte

nent and the shear banding in this component increase. For medium rolling degrees (about 70%), where the change of the rolling texture development (lath to pancake model) was found to take place, the development of {111}⟨112⟩ stops and, moreover, the shear bands rotate into rolling direction, so that the amount of Goss even decreases again.

This interpretation is supported by the fact that a high amount of carbon in solution (figure 13a) enhances the formation of Goss orientation, whereas in the case of precipitated carbon (figure 13b), the orientation density of Goss is strongly reduced. The reason seems to be that carbon in solution leads to more deformation inhomogeneities like shear bands[3)–5)]. In agreement also in additional investigations of interstitial-free Ti bearing steels where the whole content of carbon is precipitated no Goss orientations could be observed. The same effect as well for shear

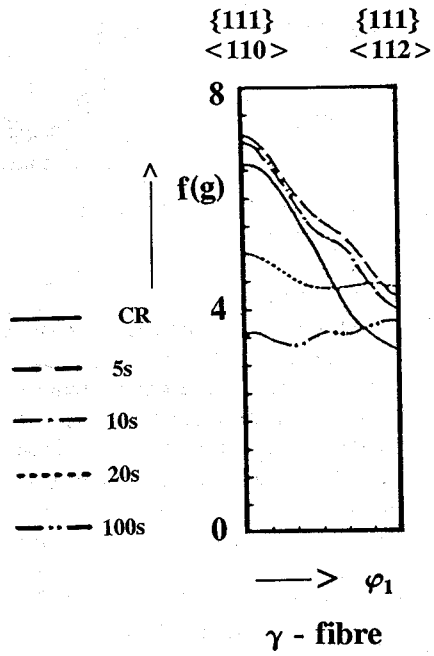


**Figure 15.** $\gamma$-fibre of cold-rolled and annealed sample, $T$ = 700 °C

**Bild 15.** $\gamma$-Faser der kaltgewalzten und geglühten Probe, $T$ = 700 °C

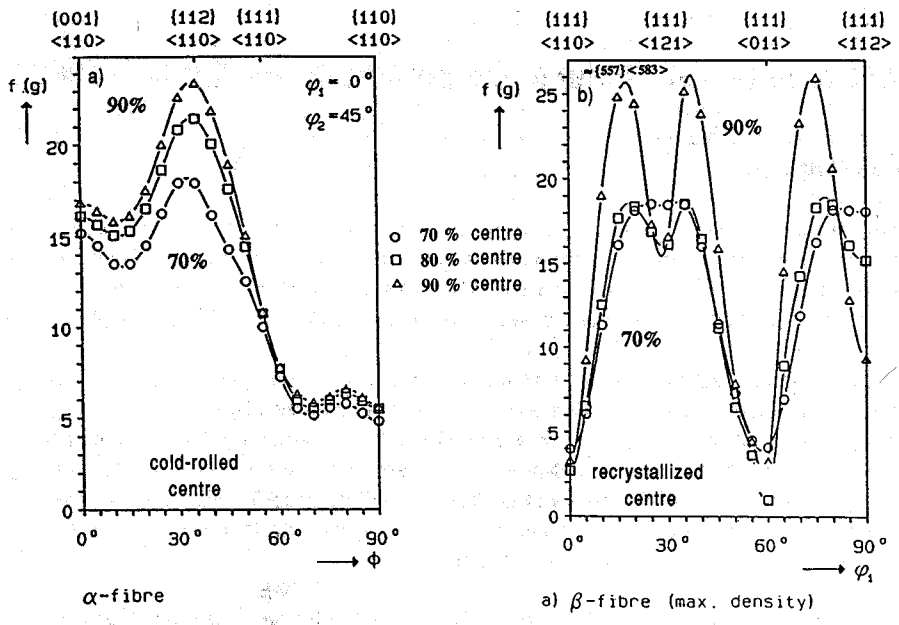


**Figure 16a.** Cold-rolling texture, center, Ti-microalloyed Fe-17%Cr steel

**Bild 16a.** Kaltwalztextur in der Probenmitte, Ti-mikrolegierter Fe-17%Cr-Stahl

**Figure 16b.** Recrystallization texture of a Ti-microalloyed Fe-17%Cr steel of several rolling degrees

**Bild 16b.** Rekristallisationstextur eines Ti-mikrolegierten Fe-17%Cr-Stahles über dem Walzgrad

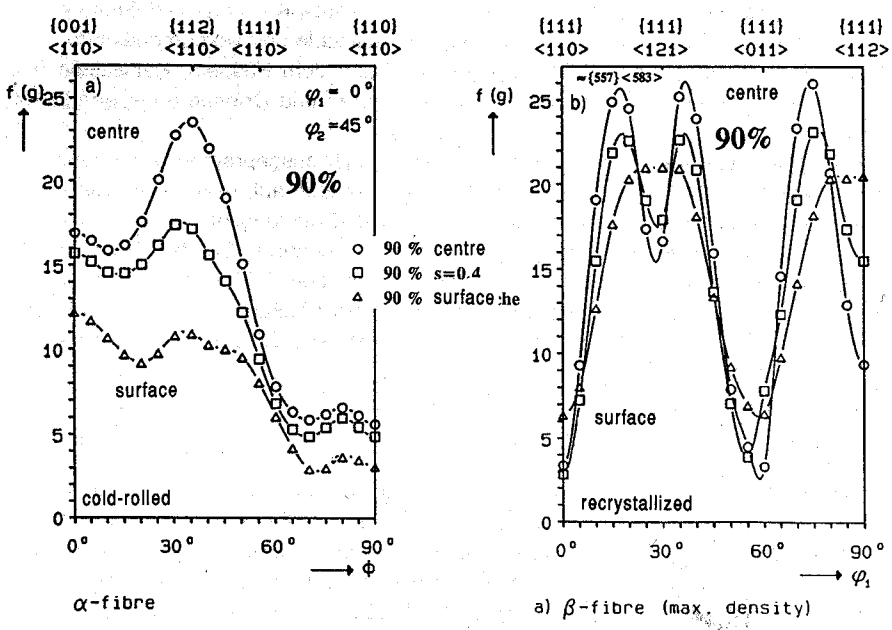


**Figure 17a.** Cold-rolling texture of a microalloyed Fe-17%Cr steel, $\varepsilon$ = 90%

**Bild 17a.** Kaltwalztextur über der Schichtdicke, Ti-mikrolegierter Fe-17%Cr-Stahl, $\varepsilon$ = 90 %

**Figure 17b.** Recrystallization texture of a Ti-microalloyed Fe-17%Cr of three different layers, $\varepsilon$ = 90%

**Bild 17b.** Rekristallisationstextur eines Ti-mikrolegierten Fe-17%Cr-Stahles über der Schichtdicke, $\varepsilon$ = 90 %

band formation as for the high density of Goss may be reached by increasing initial grain size.

At the surface (figure 14a) larger grains exist and, therefore, a strong-$\eta$-fibre is formed by recrystallization. In the center layer the hotband microstructure consists of very thin elongated grains in which no shear band formation and thus no $\eta$-fibre occurs (figure 14b). Here the strong rolling texture compoenent {112}⟨110⟩ effects a very strong recrystallization orientation {111}⟨112⟩ or {557}⟨583⟩ as already pointed out.

(A 00 595; received: 3. July 1991)

## References


1) *Hölscher, M.:* Walz- und Rekristallisationstexturentwicklung ferritischer Stähle, insbesondere von Fe16%Cr. Dr.-Ing.-Diss. RWTH Aachen (1987).

2) *Bunge, H. J.:* "Mathematische Methoden der Texturanalyse", Akademie-Verlag, Berlin (1969).

3) *Därmann, C.; Hölscher, M.; Mishra, S.; Lücke, K.:* Proc. ICOTOM 7, Netherlands, p. 759 (1984).

4) *Därmann, C.:* Entwicklung der Textur und Mikrostruktur bei der Verformung und Rekristallisation von Fe3%Si. Dr.-Ing.-Diss. RWTH Aachen (1983).

5) *Schlippenbach, U. v.; Emren, F.; Lücke, K.:* Acta metall. 34 (1986), p. 1289.

6) *Taylor, G. I.:* J. Inst. Met. 62 (1938), p. 307.

7) *Bishop, J. F. W.; Hill, R.:* Phil. Mag. 42 (1951), p. 1298.

8) *Honneff, H.:* Berechnung der Orientierungsänderungen und Texturentwicklung beim Walzen kristalliner Festkörper mit Hilfe eines modifizierten Taylor-Modells. Dr.-Ing.-Diss. RWTH Aachen (1980).

9) *Fortunier, R.; Hirsch, J.:* "Theoretical Techniques of Texture Analysis", [ed.:] H. J. Bunge, DGM-Verlag (1986).

10) *Dillamore, I. L.; Katoh, H.:* Met. Sci. 8 (1974), p. 21.

11) *Backofen, W. A.; Hundry, B. B.:* Trans. AIME 197 (1953), p. 51.

12) *Ibe, G.; Lücke, K.:* Arch. Eisenhüttenwes. 39 (1968), p. 693.

13) *Avraamov, Y.; Grozdev, A.; Kutsak, V.:* Fiz. metal. metallored. 36 (1973) No. 5, p. 1108/111.

14) *Hutchinson, W. B.:* Proc. ICOTOM 8, [eds.:] J. Kallend and G. Gottstein, The met. society (1988), p. 603/12.

15) *Raabe, D.; Lücke, K.:* to be published.

16) *Lücke, K.:* Canad. Metal. Quart. 13 (1974), p. 261/74.